J. Fluid Mech. (2008), *vol.* 611, *pp.* 427–442.
doi:10.1017/S0022112008003030 Printed in the United Kingdom

Evolution of nonlinear processes in a hypersonic boundary layer on a sharp cone

D. BOUNTIN, A. SHIPLYUK AND A. MASLOV

Khristianovich Institute of Theoretical and Applied Mechanics, Russian Academy of Sciences, Novosibirsk, 630090, Russia

(Received 6 October 2006 and in revised form 17 June 2008)

Nonlinear processes in a hypersonic boundary layer on a sharp cone are considered using the bicoherence method. The experiments are performed for a Mach number $M_\infty = 5.95$ with introduction of artificial wave packets at the frequency of the second mode. It is shown that the basic mechanism of nonlinear interaction at the location of the maximum r.m.s. voltage fluctuation is the subharmonic resonance; all nonlinear interactions in the maximum r.m.s. voltage fluctuation layer are related to the second mode of disturbances; nonlinear processes above and below that layer are much more intense than those in it. The effect of artificial disturbances on nonlinear interactions in the boundary layer is shown to be insignificant.

1. Introduction

The study of the boundary-layer transition to turbulence is of particular importance at high speeds as the skin friction and thermal loads on an air vehicle significantly depend on the boundary-layer flow state. In the case of low-level free-stream disturbances (i.e. for in-flight conditions), the transition of the boundary layer is assumed to be due to the growth of boundary-layer disturbances and their subsequent nonlinear interactions. The dominating type of disturbance in a hypersonic boundary layer beginning from $M \approx 4$ is the second mode or the Mack mode, so called since it was first theoretically identified by Mack in 1969. In contrast to the first vortical mode or instability of the type of Tollmien–Schlichting waves, the second mode has an acoustic nature and is an inviscid instability. The first experimental detections of the second mode were made by Kendall (1975), Demetriades (1978), and Stetson *et al.* (1983).

Nonlinear interaction of the boundary-layer disturbances leads to the formation of phase-coupled waves, which results in transition to turbulence of the laminar flow, manifested, in particular, in a redistribution of spectral energy. It was found that the basic type of nonlinear interaction in a subsonic boundary layer at the initial stage of its transition is the subharmonic (parametric) resonance of the Tollmien–Schlichting waves (Kachanov & Levchenko 1984; Saric, Koslov & Levchenko 1984). This type of three-wave interaction involves nonlinear amplification of disturbances whose frequency equals half of the frequency of the fundamental wave (subharmonic). Kosinov *et al.* 1994 showed that subharmonic resonance is also the main mechanism of interaction in the weakly nonlinear region of the transition in a supersonic boundary layer. In contrast to the subsonic case, resonance interaction at supersonic velocities occurred for an asymmetric wave triad.

Detailed research on nonlinear processes at subsonic and moderate supersonic velocities ($M < 4$) became possible due to the development of the method of artificial wave packets (Kachanov, Gilyev & Kozlov 1983; Maslov, Kosinov & Shevelkov 1990). Application of this method at hypersonic velocities is rather difficult. Nonlinear processes can be studied without the introduction of artificial fluctuations by the statistical method and by the bicoherence method. In the statistical method, the existence of nonlinearity is determined by signal deviation from the Gaussian distribution (Papoulis 1965; Nikias & Raghuveer 1987). The statistical method also has some drawbacks: it does not allow the obtaining of particular characteristics of the nonlinear process. To determine, in addition to mere identification of the nonlinearity, which waves are nonlinearly coupled and the degree of this coupling, one has to measure signal bicoherence (for quadratic nonlinearity only). As applied to processes in hypersonic boundary layers, this method was first used by Kimmel & Kendall (1991) to analyse data obtained for a sharp cone with a half-angle of 7° and $M_\infty = 8$ and later by Chokani (1999) to analyse data obtained in the quiet wind tunnel NASA LaRc Mach-6 for a sharp cone with a pressure gradient. It was shown in their experiments that the second mode harmonic observed in signal spectra is the result of nonlinear interaction (harmonic resonance). The existence of subharmonic resonance in a hypersonic boundary layer on a sharp cone was first demonstrated by Shiplyuk *et al.* 2003(*a*). Interaction of the second mode with natural and artificial disturbances was considered by Shiplyuk *et al.* 2003(*b*). The influence of a porous surface on the disturbance evolution and their nonlinear interactions in a hypersonic boundary layer can be found in Chokani *et al.* (2005).

In all the above-mentioned experiments at hypersonic speeds nonlinear investigations were carried out in the layer of the maximum r.m.s. voltage fluctuation. In addition to nonlinear interactions in the layer of the maximum fluctuation, the present work deals with nonlinear processes above and below it. The influence of artificial disturbances on nonlinear interactions in the boundary layer is also analysed.

2. Experimental equipment

The experiments are performed in the T-326 hypersonic blowdown wind tunnel of the Khristianovich Institute of Theoretical and Applied Mechanics of the Siberian Branch of the Russian Academy of Sciences (ITAM SB RAS) at a free-stream Mach number $M_\infty = 5.95$, stagnation pressure $P_0 = 10^6$ Pa, and stagnation temperature $T_0 = 390$ K, which yield a free-stream Reynolds number $Re_{1\infty} = 12 \times 10^6\, m^{-1}$ and the Reynolds number based on boundary-layer-edge values $Re_{1e} = 15.8 \times 10^6\, m^{-1}$. The values of the parameters P_0 and T_0 are maintained constant during the experiment within 0.06 % and 0.25 %, respectively. The free-stream parameters M_∞ and $Re_{1\infty}$ are determined from the measured values of P_0 and T_0 and from the known dependence $M_\infty = f(P_0)$ obtained by studying the flow field in the T-326. The test section of the tunnel is open-jet test section 400 mm in length having a core flow diameter of 180 mm. The fluctuations of the mass flow ρu (ρ is the flow density and u is the flow velocity) are measured by a constant-current hot-wire anemometer with a frequency range up to 600 kHz. Single-wire probes 1 mm long are used; the probes are made from a tungsten wire 5 μm in diameter. The position accuracy of the hot-wire probe across the boundary layer is 0.01 mm. The x coordinate is taken from the model tip along the cone generatrix (figure 1); the accuracy of motion along the x-axis is 0.02 mm. The model is rotated around its centreline within 0.1°.

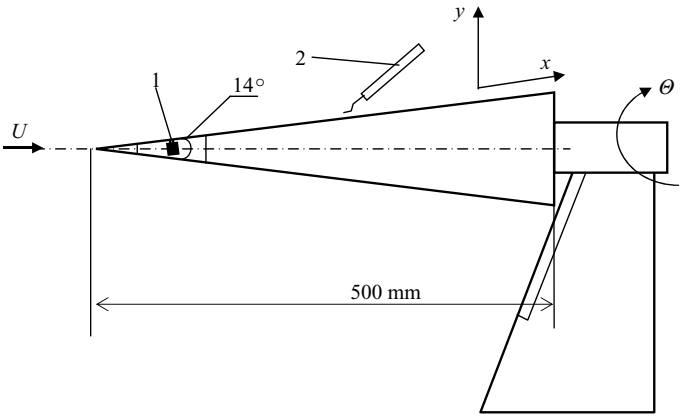

FIGURE 1. Schematic of the model. 1 – glow discharge source (GDS); 2 – hot-wire gauge.

The variable component of the electric signal from the hot-wire output is transferred into a PC memory through a 12-bit analog-to-digital converter. The anemometer output voltage is sampled at 5 MHz, which yields Nyquist frequency 2.5 MHz. As the frequency bandwidth of the hot wire is limited, the data used are from the range up to 600 kHz only.

The model is a 7° half-angle steel cone 0.5 m long and sharp nosed. The bluntness radius of the model tip is smaller than 0.1 mm. The model is mounted at zero incidence with an accuracy of 0.06°. To excite artificial disturbances in the boundary layer, the model is equipped with a glow discharge source (GDS). The operation of this device is based on the high-frequency electric glow discharge in a chamber beneath the model surface. This technique is widely used at ITAM to insert artificial disturbances into supersonic and hypersonic boundary layers (see e.g. Fedorov *et al.* 2003). Periodic oscillations penetrate into the boundary layer through an orifice 0.4 mm in diameter, which is located at $x = 120$ mm. The GDS is driven by high-voltage unidirectional periodical pulses with amplitudes up to 700 V. The frequency of artificial disturbances is 290 kHz, which is in the second-mode frequency band in the present conditions. For the model to be under adiabatic conditions, the stagnation temperature at the beginning of the run is increased to $T_0 \approx 500$ K, and the model is heated within several minutes to the recovery temperature $T_r \approx 330$ K.

3. Statistical and bispectral analysis

To identify the effects of nonlinearity, the known fact that a Gaussian signal passing through a nonlinear system deviates from the normal distribution is used (Papoulis 1965; Nikias & Raghuveer 1987). To determine this deviation, skewness $S = \mu_3/\sigma^3$ and kurtosis $K = \mu_4/\sigma^4$ are calculated, where $\mu_3 = \mathrm{E}\{(v\text{-}v_{mean})^3\}$ is the third-order central moment, $\mu_4 = \mathrm{E}\{(v\text{-}v_{mean})^4\}$ is the fourth-order central moment, $\sigma^2 = \mathrm{E}\{(v\text{-}v_{mean})^2\}$ is the variance, $v_{mean} = \mathrm{E}\{v\}$ is the mean value, and $\mathrm{E}\{\}$ is the expected value. For the Gaussian distribution, $S = 0$ and $K = 3$.

A significant drawback of this method is that it does not yield particular characteristics of the nonlinear process. One has to apply a bispectral analysis to not merely obtain the effect of nonlinearity but also to determine which waves are nonlinearly coupled and the degree of this coupling (or the degree of nonlinear interaction). The bispectrum is obtained by a Fourier transform applied to the

third-order cumulant (or moment because cumulants and moments are identically equal up to the third order inclusive) (Nikias & Raghuveer 1987; Kim & Powers 1979)

$$B(f_1,\ f_2) = \sum_{k,l} c_3(k,l)\mathrm{e}^{-\mathrm{i}2\pi(f_1 k + f_2 l)} = \mathrm{E}\{V^*(f_1+f_2)V(f_1)\,V(f_2)\},$$

where $c_3(k,l) = \mathrm{E}\{v(t)v(t+k)v(t+l)\}$ is the third-order cumulant (moment) and V is the Fourier transform of the signal $v(t)$; the asterisk denotes the complex conjugate.

In contrast to the power spectrum, the bispectrum retains information about the wave phase, which allows one to identify phase-coupled waves. The bispectrum value depends on the wave amplitude; hence, it is usually normalized to obtain the bicoherence:

$$bic^2(f_1,\ f_2) = \frac{|B(f_1,\ f_2)|^2}{E\{|V(f_1)V(f_2)|^2\}E\{|V(f_1+f_2)|^2\}}.$$

The bicoherence amplitude characterizes the degree of quadratic phase coupling of waves with frequencies f_1, f_2, and $f_3 = f_1 + f_2$. With such normalization, bicoherence is bound by 0 (completely independent waves) and 1 (completely coupled waves); however, the value of the bicoherence is also dependent on the signal-to-noise ratio of the measured data. Thus, if the bicoherence is greater than zero for the frequency components f_1 and f_2, the triad of waves with frequencies f_1, f_2, and $f_3 = f_1 + f_2$ is phase coupled. Cubic nonlinearity or four-wave interaction are analysed with the use of trispectra determined via the fourth-order cumulant.

By virtue of the bicoherence symmetry, it suffices to know its value in the triangular region defined by the vertices $(0, 0)$, $(f_N, 0)$, $(f_N/2,\ f_N/2)$, where f_N is the Nyquist frequency. In the present paper, the figures are plotted in the range $0 < f_1,\ f_2 < 600$ kHz (the upper limit is due to the frequency range of the hot-wire anemometer) and offer redundant information (the graphs are symmetric about the line $f_1 = f_2$). However, in our opinion, such a presentation improves data perception. The bicoherence does not reveal which interaction occurs: $f_3 - f_1 \rightarrow f_2$, $f_3 - f_2 \rightarrow f_1$, or $f_1 + f_2 \rightarrow f_3$, i.e. bicoherence cannot indicate which of the three waves is generated owing to nonlinear processes. Correct interpretation of data requires additional information (e.g. the Fourier spectrum of the signal).

Bicoherence is obtained from non-overlapping FFT blocks of length 512; the frequency resolution of the bicoherence is 9.8 kHz.

4. Experimental results

4.1. *Evolution of nonlinear interactions at the maximum r.m.s. disturbance location*

Figure 2 shows the evolution of the Fourier spectra of the signal obtained at the maximum r.m.s. disturbance location on a sharp cone at the centre of the artificial wave packet. The spectra clearly show the first ($f \approx 50$–220 kHz) and second ($f \approx 230$–380 kHz) modes. The peak corresponding to the second mode is seen to be shifted toward low frequencies in the downstream direction. The reason is that the wavelength of the second mode is tuned to the boundary-layer thickness (approximately twice the boundary-layer thickness, Stetson *et al.* 1983). The figure also shows the peak at a frequency of 290 kHz corresponding to the artificial disturbances. The injected disturbances have low amplitude, but much higher than that of the oscillations of the first and second modes in the spectrum. The reason is multiple averaging of disturbance spectra (approximately 100 times). To retain information on natural

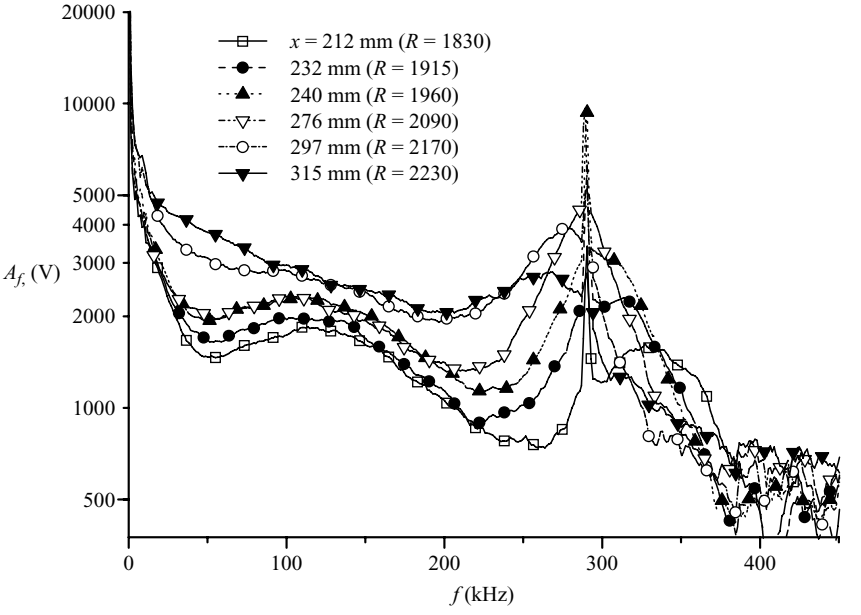

FIGURE 2. Fourier spectra evolution in the maximum r.m.s. voltage fluctuation layer at the centre of an artificial wave packet.

and artificial oscillations, the spectra are averaged as random quantities, i.e. the squared amplitudes of the Fourier spectra are averaged. As the amplitude of artificial disturbances is approximately identical for different times and the amplitude of natural oscillations is rather scattered because the process itself is random, artificial oscillations can be identified in signal spectra after averaging.

The disturbances of the first and second mode increase up to the stability Reynolds number $R = \sqrt{Re_{1e}x} = 2170$ ($x = 297$ mm), and then redistribution of the spectral energy is initiated by strong nonlinear processes: the spectrum becomes more uniform, and the second-mode amplitude decreases.

Figure 3(a) shows typical nonlinear interactions at the maximum r.m.s. disturbance location. Measurements were carried out at the centre of the wave packet. The dot-and-dashed line in the figure is the axis of symmetry of the graph, the solid line shows the equation $f_1 + f_2 = f_{II}$, where f_{II} is the frequency of the local maximum in the Fourier spectrum corresponding to the second mode. In each plot the Fourier spectrum is shown above and to the right of the plot of the bicoherence; this facilitates the interpretation of the peaks identified in the bicoherence.

Interactions occur in three frequency regions:

1. $(f_1, f_2) = (300\,\text{kHz}, 300\,\text{kHz}) \approx (f_{II}, f_{II})$. Hence, the nonlinear mechanism generates harmonics of the second-mode waves: $(f_1 \approx f_{II}) + (f_2 \approx f_{II}) \rightarrow (f_3 = f_1 + f_2 \approx 2f_{II})$. This type of interaction was previously found by Kimmel & Kendall 1991 and Chokani 1999.

2. Along the line $f_1 \approx 295$ kHz. The interacting waves have frequencies $f_1 \approx 280$–310 kHz and $f_2 \approx 50$–150 kHz. The first interval of frequencies lies in the region of the second-mode maximum in the Fourier spectrum, and the second interval of frequencies almost completely covers the frequency range corresponding to the first mode.

3. In a wide frequency range along the line $f_1 + f_2 = f_{II} \approx f_0$.

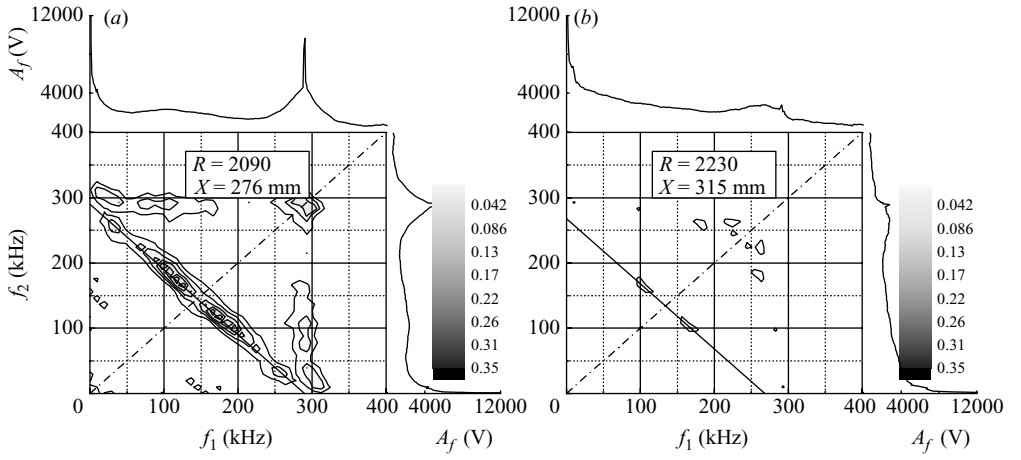

FIGURE 3. Bicoherence in the maximum r.m.s. voltage fluctuation layer at the centre of an artificial wave packet. The dot-dashed line is the axis of symmetry of the graph; the solid line shows the equation $f_1 + f_2 = f_{II}$.

Third type of nonlinear interaction involves the waves f_1, f_2, $f_3 = f_1 + f_2 \approx f_{II} \approx f_0$. The centre of interaction is $(f_1, f_2) \approx (125\,\text{kHz}, 175\,\text{kHz})$, $f_3 = f_1 + f_2 = 300\,\text{kHz} \approx f_{II} \approx f_0$. The frequency 125 kHz might appear because it is close to the frequency of the local maximum in the Fourier spectrum corresponding to the first mode ($f_I \approx 120\,\text{kHz}$). It should be noted that the frequencies of 125 and 175 kHz are close to the frequency of the second-mode subharmonic (at this station, $1/2\,f_{II} \approx 155\,\text{kHz}$). This type of nonlinear interaction in hypersonic boundary layers was first obtained by Shiplyuk *et al.* (2003*a*). Identification of waves close to the second-mode subharmonic and synchronized with the fundamental wave is a necessary condition of subharmonic resonance with detuning. Thus, the following conditions have to be satisfied for the parametric three-wave resonance to exist in the general case (Craik 1971):

$$f_1 + f_2 = f_3, \quad \alpha_1 + \alpha_2 = \alpha_3, \quad \beta_1 + \beta_2 = \beta_3 \tag{1}$$

(α and β are the streamwise and transverse wavenumbers).

From the definition of bicoherence, we obtain

$$f_1 + f_2 = f_3 \approx f_{II}, \quad \varphi_1 + \varphi_2 = \varphi_3, \tag{2}$$

where φ is a phase. The first equality is identical for both cases. Taking into account that $\varphi = \alpha x + \beta z$, the second equality in (2) can be rewritten as

$$\alpha_1 x + \beta_1 z + \alpha_2 x + \beta_2 z = \alpha_3 x + \beta_3 z,$$
$$(\alpha_1 + \alpha_2)x + (\beta_1 + \beta_2)z = \alpha_3 x + \beta_3 z.$$

Waves of the second mode are two-dimensional (Poggie & Kimmel 1997; Maslov *et al.* 2006), i.e. $\beta_3 = \beta_{II} = 0$, and waves close to the subharmonic are three-dimensional because they lie in the range of the first-mode disturbances; hence, as was shown in our previous experiments (Maslov *et al.* 2006), subharmonic oscillations consist of a pair of oblique waves with $\beta_1 = -\beta_2$. Thus, we obtain

$$\alpha_1 + \alpha_2 = \alpha_3. \tag{3}$$

All resonance conditions are satisfied. This interaction resembles the subharmonic resonance observed at subsonic velocities (Kachanov & Levchenko 1984) where the disturbances of the fundamental wave are also two-dimensional, and the subharmonic waves form a pair of oblique waves. As the subharmonic frequency lies in the range corresponding to the first-mode oscillations, which is noted above, apparently the interaction between the modes occurs here.

The presence of a wide frequency range of interacting waves and identification of a frequency not completely coincident with the subharmonic frequency do not contradict the existence of the resonance. In the case of subsonic velocities, subharmonic resonance exists with a frequency detuning $f_{1/2} \pm \Delta f$ up to $\Delta f = f_{1/2}$ (Kachanov & Levchenko 1984), and phase synchronism of waves participating in the resonance is observed in a wide range of frequencies up to the fundamental-wave frequency f_0 (Borodulin, Kachanov & Koptsev 2002). It is of interest to note that in the second interaction type (along the line $f_1 \approx 295\,\mathrm{kHz}$) the frequency of the third interacting wave $(f_1 \approx 100\,\mathrm{kHz}) + (f_2 \approx 300\,\mathrm{kHz}) \rightarrow (f_3 = f_1 + f_2 = 400\,\mathrm{kHz})$ roughly corresponds to the spectral component $\frac{3}{2} f_{1/2} \approx 430\,\mathrm{kHz}$ often observed in subharmonic resonance at subsonic velocities (Kachanov 1994).

Nonlinear interaction along the line $f_1 + f_2 = f_{II}$ can also be found in Kimmel & Kendall (1991), but this type of interaction was much weaker than interaction leading to the generation of the second-mode harmonic, and we did not consider it.

As the initial stage of nonlinear interaction is similar to that observed at subsonic velocities, the later stages of the transition in a hypersonic boundary layer can also be expected to be similar to the case of subsonic velocities. Indeed, the computations of Adams & Kleiser (1996) showed that the late stage of the nonlinear region of the transition gives rise to structures that resemble Λ-vortices observed in subsonic boundary layers. The computations were performed by means of direct numerical simulations for a flow with $M = 4.5$ past a flat plate. Subharmonic resonance was set as a nonlinear interaction mechanism.

The quadratic-type nonlinear processes almost disappear at the last station (figure 3*b*). It is seen from figure 2 ($R = 2230$, $x = 315\,\mathrm{mm}$), however, that the Fourier spectrum of the signal becomes close to turbulent at this location owing to nonlinear interactions, which can be inferred from a more uniform shape of the spectrum. As will be shown in § 4.2, strongly nonlinear processes occur below and above the layer of the maximum r.m.s. voltage fluctuation, which seem to be responsible for the spectral energy redistribution.

Some other details of the evolution of nonlinear interactions at the maximum r.m.s. disturbance location are given in Shiplyuk *et al.* (2003*b*).

4.2. *Nonlinear processes across the boundary layer*

In this Section, a nonlinear analysis of data measured by a hot wire at the centre of an artificial wave packet across the boundary layer is performed. The boundary-layer measurements are carried out at four stations: $R = 1480$ ($x = 138\,\mathrm{mm}$), $R = 1820$ (209 mm), $R = 1970$ (245 mm), and $R = 2230$ (315 mm).

At the first location $R = 1480$, the kurtosis K corresponds to the Gaussian distribution ($K \approx 3$, figure 4*b*). Except for a small region $y/\delta = 0.751$–1, the skewness S is also consistent with the normal distribution ($S \approx 0$, figure 4*b*). For $y/\delta = 0.751$–1, the skewness is slightly different from zero, which is indicative of weak nonlinear processes. Profiles of the mean voltage E and root-mean-square fluctuations of voltage $\langle e \rangle$ on the hot-wire probe are shown in figure 4(*a*). The y coordinate is normalized

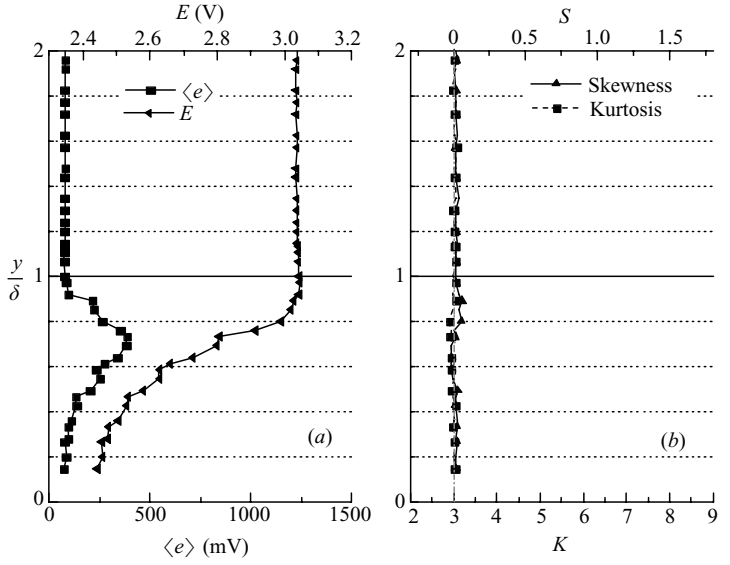

FIGURE 4. (*a*) Mean voltage E and root-mean-square fluctuations of voltage $\langle e \rangle$ on the hot-wire probe (*b*); skewness S and kurtosis K. $R = 1480$ ($x = 138$ mm).

to the boundary-layer thickness δ. The peak in the distribution of $\langle e \rangle$ shows the layer of the maximum r.m.s. voltage fluctuation.

The bicoherence shows that no phase-coupled waves are observed in the boundary layer (figure 5*a*, $y/\delta = 0.75$) at this location up to the layer of the maximum r.m.s. voltage fluctuation ($y/\delta \approx 0.7$, figure 4*a*) and higher. The dashed line shows the equation $f_1 + f_2 = f_0$, where f_0 is the frequency of artificial disturbances. In the region where S differs from zero in the low-frequency range (up to ~ 50 kHz), however, the bicoherence shows the presence of nonlinear interactions and reaches the maximum value near the upper edge of the boundary layer (figure 5*b*, $y/\delta = 0.97$). In the free flow (figure 5*c*, $y/\delta = 1.05$), phase coupling disappears again. The Fourier spectra of the signal display a moderate peak at the frequency of artificial disturbances ($f = 290$ kHz), which disappears toward the boundary-layer edge. Neither the first nor the second modes can be identified in the signal spectra yet.

The presence of nonlinear processes at the boundary-layer edge at the station where the flow is definitely laminar can be related to aerodynamic noise in the T-326 wind tunnel, which is not a quiet tunnel. The level of free-stream mass flux pulsation is about 0.5 % of mean mass flux. Thus, high-amplitude disturbances present in the free flow and incident on the boundary layer can initiate weak nonlinear interactions at the boundary-layer edge. However, at the next stations nonlinear interactions near the boundary-layer edge have a wider spectrum and the bicoherence amplitude becomes higher. This shows that at downstream locations the nonlinear mechanism is related to inner processes of boundary layer, but not to free-stream noise. Otherwise, the interaction frequency range and interaction intensity would not be changed, because the free-stream noise spectrum and amplitude are the same for all stations. Nonlinear processes above the maximum r.m.s. disturbance can also be a result of a mixture of different nonlinear mechanisms.

At the next station $R = 1820$ (209 mm), the skewness noticeably deviates from zero toward positive values in the region above the layer of the maximum r.m.s. voltage

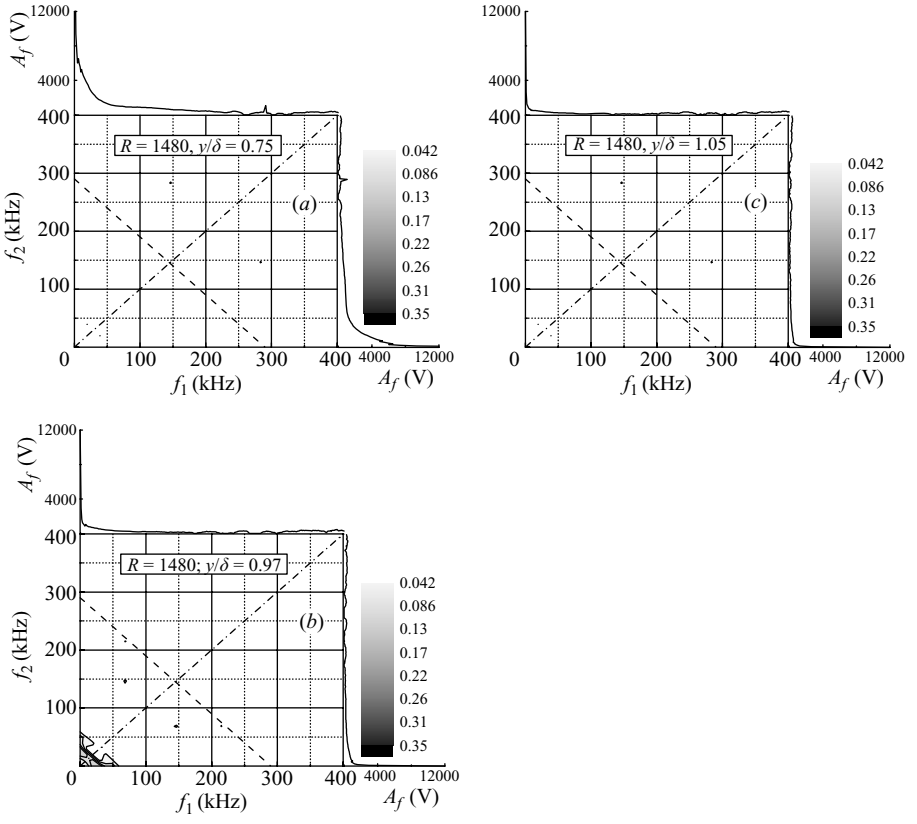

FIGURE 5. Bicoherence and Fourier spectra (above and to the right) across boundary layer. $R = 1480$ ($x = 138$ mm).

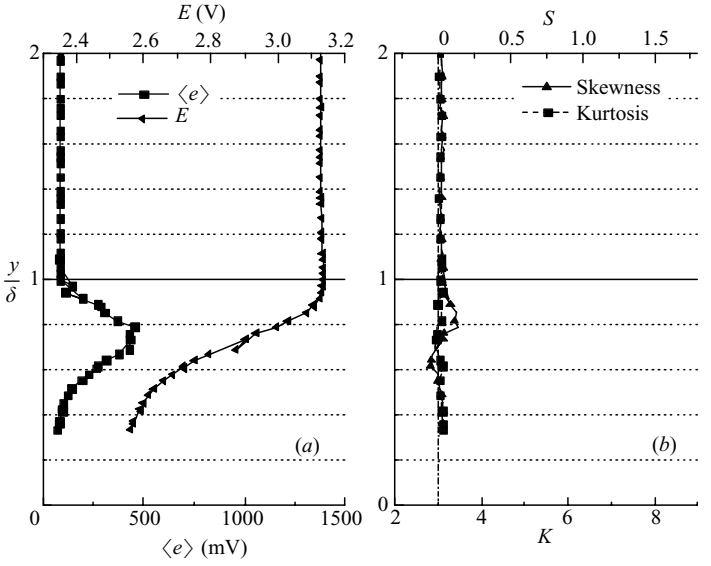

FIGURE 6. (*a*) Mean voltage E and root-mean-square fluctuations of voltage $\langle e \rangle$ on the hot-wire probe (*b*) skewness S and kurtosis K. $R = 1820$ ($x = 209$ mm).

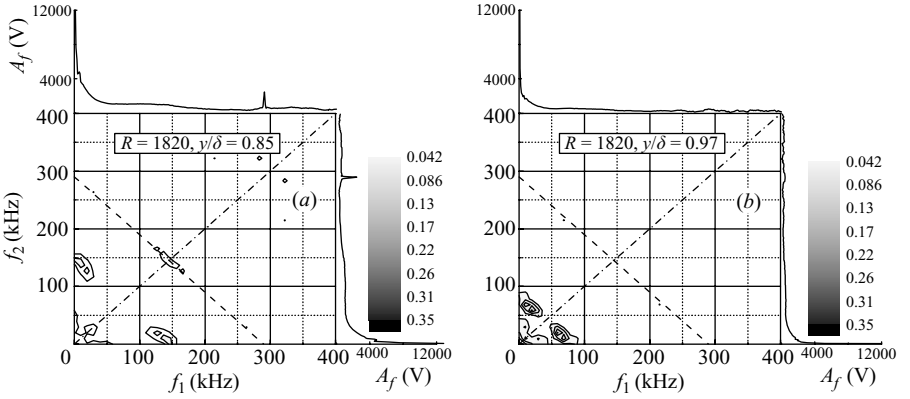

FIGURE 7. Bicoherence and Fourier spectra across boundary layer. $R = 1820$ ($x = 209$ mm).

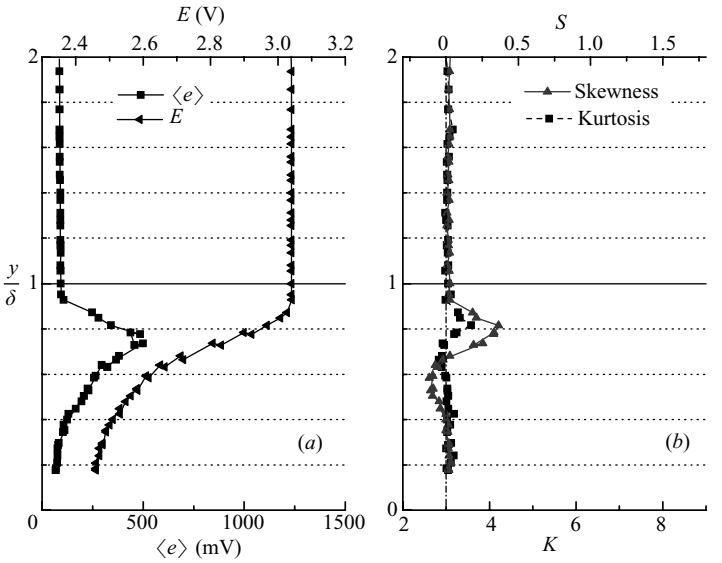

FIGURE 8. (*a*) Mean voltage E and root-mean-square fluctuations of voltage $\langle e \rangle$ on the hot-wire probe (*b*) skewness S and kurtosis K. $R = 1970$ ($x = 245$ mm).

fluctuation and toward negative values in the region below that layer (figure 6*b*). This deviation disappears near the boundary-layer edge. It is of interest to note that the skewness in the layer of the maximum r.m.s. voltage fluctuation is close to the value of the normal distribution. The kurtosis equals 3 across the entire boundary layer and outside it.

The bicoherence shows that there are nonlinear processes above the layer of the maximum r.m.s. voltage. In addition to interactions at low frequencies, which have already been observed at $R = 1480$, a weak interaction arises along the line $f_1 + f_2 = f_0$ (figure 7*a*, $y/\delta \approx 0.85$). As at the previous station, the bicoherence reaches the maximum amplitude near the boundary-layer edge (figure 7*b*, $y/\delta = 0.97$). The range of nonlinear interaction at low frequencies becomes wider: $f \leqslant 100$ kHz. The peak at the frequency of artificial disturbances in the Fourier spectra becomes higher (figure 7*a*). Nonlinear interactions vanish outside the boundary layer.

At the station R = 1970 (245 mm), the skewness deviations toward negative values below the maximum r.m.s. voltage fluctuation layer and toward positive values above it become much more noticeable (figure 8*b*), i.e. nonlinear interactions become more intense. The deviation of the kurtosis is also noticeable at this station. As the kurtosis is determined via the fourth-order moment related to trispectra, nonlinear interactions of the third order apparently start contributing to the process here (Nikias & Raghuveer 1987). Qualitatively, the kurtosis behaviour coincides with the skewness behaviour. In the region of the layer of the maximum r.m.s. voltage fluctuation, the value of K corresponds to the Gaussian distribution. The skewness line intersects the zero axis ($S = 0$) somewhat lower than the layer of the maximum r.m.s. voltage fluctuation. The free-stream values of both coefficients are consistent with the Gaussian distribution.

The bicoherence amplitude exceeds the noise level at the same height at which S starts deviating from zero (figure 9*a*, $y/\delta = 0.34$). The interaction proceeds in the low-frequency region $f \leqslant 70$ kHz. On moving upward from the model wall, the bicoherence amplitude in the low-frequency range gradually decreases; simultaneously, nonlinear processes appear along the subharmonic-resonance line (figure 9*b*, $y/\delta = 0.5$). Interaction of the second mode with low-frequency waves is most intense here ($f_1 \approx 290$ kHz, $f_2 \approx 25$ kHz, $f_3 = f_1 + f_2 \approx 315$ kHz).

In the layer of the maximum r.m.s. voltage fluctuation, nonlinear processes at low frequencies disappear, but the bicoherence amplitude along the subharmonic-resonance line increases (figure 9*c*, $y/\delta = 0.74$). Phase-coupled waves start to appear above the maximum r.m.s. voltage fluctuation layer over the entire region below the line of the basic interaction (figure 9*d*, $y/\delta = 0.82$). The interaction corresponding to the subharmonic resonance disappears toward the boundary-layer edge. There remains only the region in the low-frequency range, which is observed at the previous stations (figure 9*e*, $y/\delta = 0.93$). No nonlinear processes are observed above the boundary layer.

As expected, nonlinear interactions become more intense in the downstream direction. At the last location $R = 2230$ ($x = 315$ mm), the skewness and kurtosis deviations become much more noticeable (figure 10*b*). There are no regions in the boundary layer with K and S corresponding to the Gaussian distribution, except for the points of intersection of the lines $K = 3$ and $S = 0$. Qualitatively, the skewness and kurtosis distributions remain the same as those for $R = 1970$. The increase in the kurtosis value shows that the role of the third-order nonlinear interactions becomes more and more significant. These data differ from those measured at the previous locations in that the deviation of the values of S and K from the Gaussian distribution is extended outside the boundary layer and vanishes at the height $y/\delta = 1.55$.

Near the wall, the bicoherence displays strong nonlinear interactions in the low-frequency range (figure 11*a*, $y/\delta = 0.09$). As at the previous station, the interaction intensity at low frequencies decreases with increasing y coordinate and almost disappears in the layer of the maximum r.m.s. voltage fluctuation (figure 11*b*, $y/\delta = 0.61$). Instead, a weak interaction appears along the line $f_1 + f_2 = f_{II}$, which has been already observed previously (figure 3*b*). The amplitude of artificial disturbances is almost invisible in the Fourier spectrum of the signal (figure 11*b*). As at the previous station $R = 1970$, phase-coupled waves along the line $f_1 + f_2 = f_{II}$ disappear with increasing y, and nonlinear processes start to appear in the entire region below the subharmonic-resonance line, reaching the maximum value at the boundary-layer edge (figure 11*c*, $y/\delta = 0.98$). The bicoherence amplitude here reaches the maximum value $bic^2 = 0.43$ ($bic = 0.66$). Apparently, it is because of intense nonlinear interactions below and above the layer of the maximum r.m.s. voltage fluctuation that the Fourier spectrum becomes more smooth, which is observed on moving in the x direction

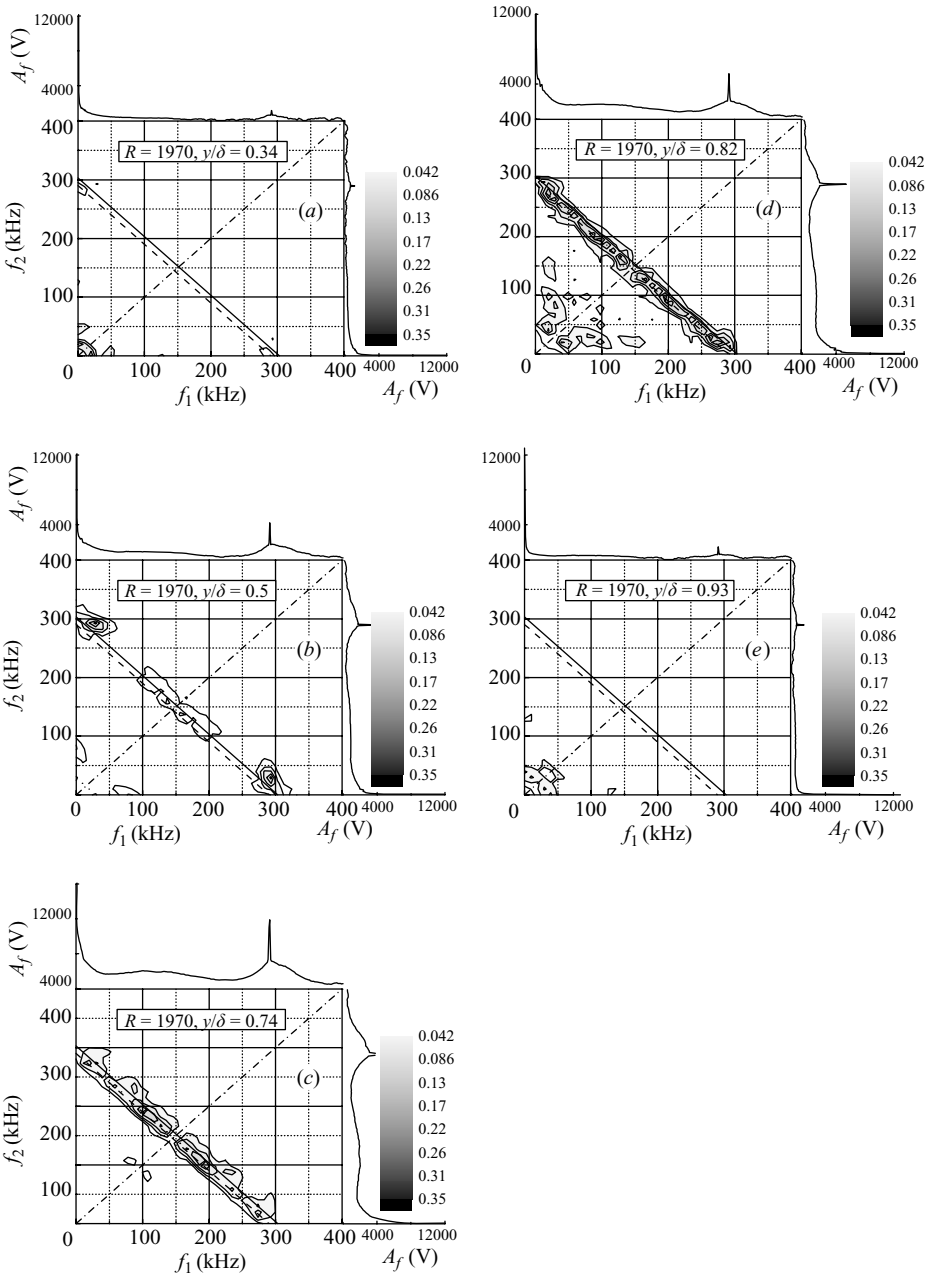

FIGURE 9. Bicoherence and Fourier spectra across boundary layer. $R = 1970$ ($x = 245$ mm).

(figure 2, $R = 2230$). Though the nonlinear processes along the subharmonic-resonance line disappear above the maximum r.m.s. voltage fluctuation layer, the interaction region is bounded by this line (figure 11*c*, $y/\delta = 0.98$), i.e. the frequency of the interacting waves is lower than f_{II}. Although the Fourier spectrum at $y/\delta = 0.98$ is smooth and shows no modes, we believe that the most likely reason for this bound is Fourier amplitude decay beyond the frequency f_{II} in the maximum r.m.s. layer. This suggests that the second mode plays an important role in nonlinear processes in a

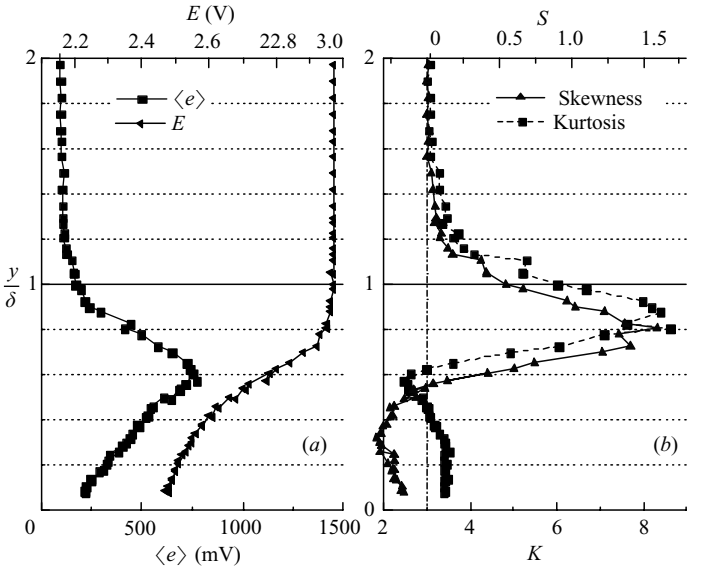

FIGURE 10. (*a*) Mean voltage E and root-mean-square fluctuations of voltage $\langle e \rangle$ on the hot-wire probe; (*b*) skewness S and kurtosis K. $R = 2230$ ($x = 315$ mm).

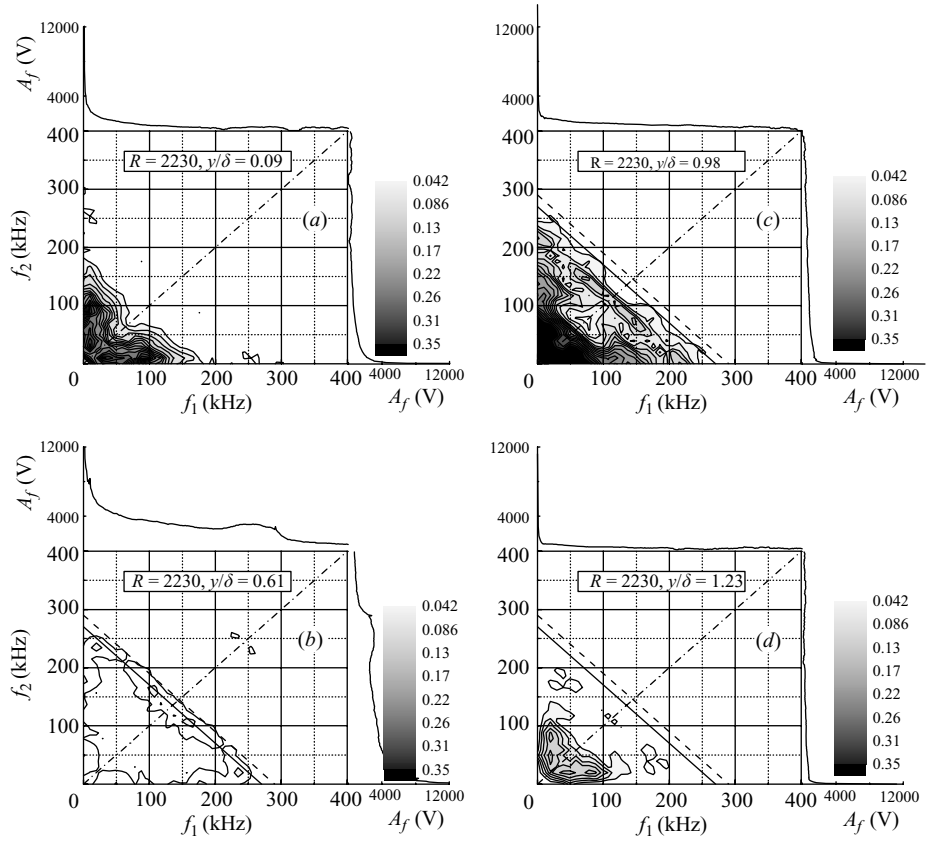

FIGURE 11. Bicoherence and Fourier spectra across boundary layer. $R = 2230$ ($x = 315$ mm).

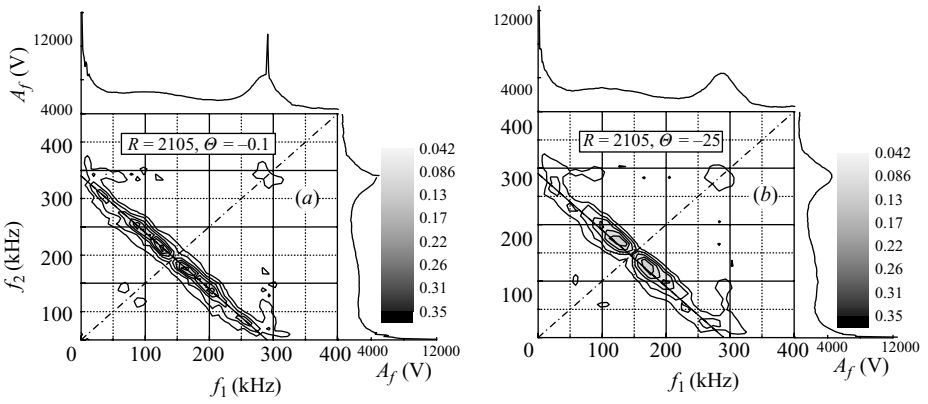

FIGURE 12. Bicoherence and Fourier spectra (a) at the centre of an artificial wave packet (b) and outside it. $R = 2105$ ($x = 280$ mm).

boundary layer. By analogy with the subsonic model of the transition to turbulence we can assume that the second mode plays a catalytic role in energy transfer from the mean flow to the low-frequency disturbances. Intensive nonlinear interactions in the low-frequency range may also indicate the appearance of coherent structures.

In contrast to the previous stations, here phase-coupled waves do not disappear out of the boundary layer (figure 11d, $y/\delta = 1.23$). Nevertheless, the region of the interacting waves decreases to 100–150 kHz, and the value of the bicoherence is lower. The bicoherence amplitude displays no nonlinear processes only at a height where the skewness takes a zero value (figure 10b, $y/\delta = 1.55$). As is seen from figure 10(a), the r.m.s. fluctuations also occur outside the boundary-layer edge. Though the plot of the mean voltage distribution does not display any distortions of the mean flow parameters at the boundary-layer edge and above, nevertheless the fact that the nonlinear processes and mass-flow fluctuations occur outside the boundary layer definitely suggests that a turbulent boundary layer starts to form.

4.3. *Effect of artificial disturbances on nonlinear processes*

The next step in a nonlinear investigation of the hypersonic boundary layer is the application of an artificial wave packets (AWP) method. It is important to show that the AWP method does not affect basic nonlinear mechanisms and can be applied in such kinds of investigations. To determine the effect of artificial disturbances on nonlinear processes in the boundary layer, the measurements are performed in the layer of the maximum r.m.s. voltage fluctuation over the angle of model revolution Θ.

Figure 12 shows the results measured at the location $R = 2105$ ($x = 280$ mm). At the centre of the wave packet (figure 12a, $\Theta = -0.1°$), the Fourier spectrum displays a high-amplitude peak corresponding to artificial oscillations, which vanishes outside the wave packet (figure 12b, $\Theta = -25°$). The nonlinear interactions follow the line $f_1 + f_2 = f_{II}$. At the centre of the wave packet and outside it, no differences in the interaction pattern are observed.

Figure 13 shows the bicoherence at the centre of the wave packet at $R = 2230$ ($x = 315$ mm) with the GDS off (figure 13a) and on (figure 13b). The operation of the source of artificial disturbances is seen to produce no effect on nonlinear processes.

Therefore, the artificial disturbances have no significant effect on the boundary layer nonlinear processes.

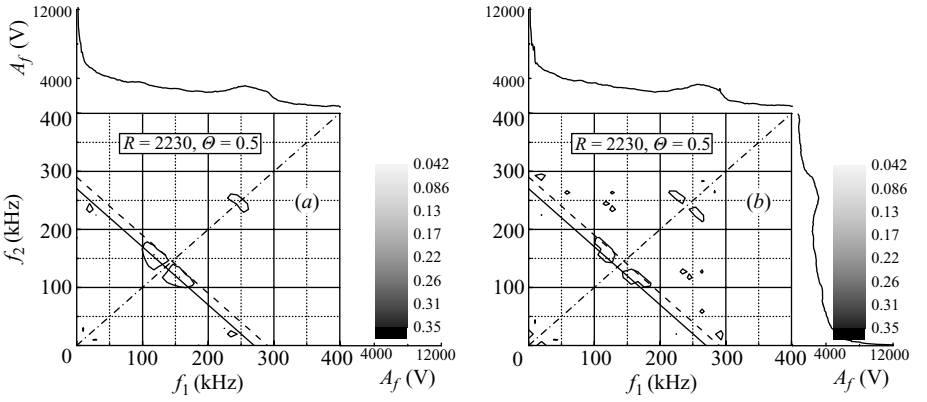

FIGURE 13. Bicoherence and Fourier spectra at the centre of an artificial wave packet with the GDS (*a*) off and (*b*) on. $R = 2230$ ($x = 315$ mm).

5. Conclusions

The initial region of the laminar–turbulent transition on a sharp cone at free-stream Mach number 5.95 has been investigated by means of a bispectral analysis.

It has been found that the main type of nonlinear interaction in the layer of the maximum r.m.s. voltage fluctuation involves interactions in a wide range of frequencies along the line $f_1 + f_2 = f_{II}$ with a maximum close to the frequency of the second-mode subharmonic, which indicates the existence of subharmonic resonance with detuning. As the second-mode subharmonic frequency belongs to the range of frequencies corresponding to the first mode of disturbances, interaction between the modes occurs here.

A nonlinear interaction leading to excitation of the second-mode harmonic, which was previously observed by other authors, is shown.

The bicoherence also shows the line of interaction ($f_1 \approx f_{II}$) of the second-mode waves with disturbances whose frequencies lie in the first-mode frequency range. Interaction between the modes can occur here as well. Thus, all basic types of nonlinear processes in the layer of the maximum r.m.s. voltage fluctuation are associated with the second mode.

Nonlinear processes at the boundary-layer edge in the range of low frequencies (up to 50 kHz) arise long before they appear in the layer of the maximum r.m.s. voltage fluctuation. Nonlinear processes in the regions above and below this layer are fairly intense even when nonlinear interactions (of the quadratic type) have almost disappeared from it. At the late stages of the transition, the nonlinear processes reach beyond the boundary layer, forming a turbulent boundary layer.

Artificial disturbances have no significant effect on the boundary-layer nonlinear processes.

The authors are grateful to Nd. Chokani for help in mastering the bispectral analysis and for useful discussions. The work was supported by the Russian Foundation for Basic Research (Grant 05-01-00349).

REFERENCES

ADAMS, N. A. & KLEISER, L. 1996 Subharmonic transition to turbulence in a flat-plate boundary layer at Mach number 4.5. *J. Fluid Mech.* **317**, 301–335.

Borodulin, V. I., Kachanov, Y. S. & Koptsev, D. B. 2002 Experimental study of resonant interactions of instability waves in self-similar boundary layer with an adverse pressure gradient. 3. Broadband disturbances. *J. Turbulence* **3**, 064.

Chokani, N. 1999 Nonlinear spectral dynamics of hypersonic laminar boundary layer flow. *Phys. Fluids.* **12**, 3846–3851.

Chokani, N., Bountin, D. A., Shiplyuk, A. N. & Maslov, A. A. 2005 Nonlinear aspects of hypersonic boundary-layer stability on a porous surface. *AIAA J.* **43**, 149–155.

Craik, A. D. 1971 Non-linear resonant instability in boundary layers. *J. Fluid Mech.* **50**, 393–413.

Demetriades, A. 1978 New experiments on hypersonic boundary layer stability including wall temperature effect. *Proc. Heat Transfer Fluid Mech. Inst.* **26**, 39–54.

Fedorov, A., Shiplyuk, A., Maslov, A., Burov, E. & Malmuth, N. 2003 Stabilization of a hypersonic boundary layer using an ultrasonically absorptive coating. *J. Fluid Mech.* **479**, 99–124.

Kachanov, U. S., Gilyev, V. M. & Kozlov, V. V. 1983 Wave space packet development in boundary layer. *Izv. Akad. Nauk USSR. Tech. Nauk.* **3**, 13 (in Russian).

Kachanov, Y. S. 1994 Physical mechanisms of laminar-boundary-layer transition. *Annu. Rev. Fluid. Mech.* **26**, 411–482.

Kachanov, Y. S. & Levchenko, V. Y. 1984 The resonance interaction of disturbances at laminar-turbulent transition. *J. Fluid Mech.* **138**, 209–247.

Kendall, J. M. 1975 Wind tunnel experiments relating to supersonic and hypersonic boundary layer transition. *AIAA J.* **13**, 290–299.

Kim, Y. C. & Powers, E. J. 1979 Digital bispectral analysis and its applications to non-linear wave interactions. *IEEE Trans. Plasma Sci.* **7**, 120

Kimmel, R. L. & Kendall, J. M. 1991 Nonlinear disturbances in a hypersonic boundary layer. *AIAA Paper* 91–0320.

Kosinov, A. D., Semionov, N. V., Shevelkov, S. G. & Zinin, O. I. 1994 Experiments on the nonlinear instability of supersonic boundary layers. In *Nonlinear Instability of Nonparallel Flows.* (ed. D. T. Valentine, S. P. Lin & W. R. C. Philips). pp 196–205. Springer.

Mack, L. M. 1969 Boundary layer stability theory. *Pasadena: Document/JPL* No. 900-277, Rev. A.

Maslov, A. A., Kosinov, A. D. & Shevelkov, S. G. 1990 Experiments on the stability of supersonic laminar boundary layers. *J. Fluid Mech.* **219**, 621–633.

Maslov, A. A., Shiplyuk, A. N., Bountin, D. A. & Sidorenko, A. A. 2006 Mach 6 boundary-layer stability experiments on sharp and blunted cones. *J. Spacecraft Rockets* **43**, 71–76.

Nikias, C. L. & Raghuveer, M. R. 1987 Bispectrum estimation: a digital signal processing framework. *Proc. IEEE* **75**, 869–891.

Papoulis, A. 1965 *Probability, Random Variables and Stochastic Processes.* McGraw-Hill.

Poggie, J. & Kimmel, R. L. 1997 Disturbance evolution and breakdown to turbulence in a hypersonic boundary layer: instantaneous structure. *AIAA Paper* 97-0556.

Saric, W. S., Kozlov, V. V. & Levchenko, V. Y. 1984 Forced and unforced subharmonic resonance in boundary layer transition. *AIAA Paper* 84-0007.

Shiplyuk, A. N., Bountin, D. A., Maslov, A. A. & Chokani, N. 2003*a* Nonlinear mechanisms of the initial stage of the hypersonic boundary layer transition. *J. Appl. Mech. Tech. Phys.* **44**, 654–659.

Shiplyuk, A., Maslov, A., Bountin, D. & Chokani, N. 2003*b* Nonlinear interactions of second mode instability with natural and artificial disturbances. *AIAA Paper* 2003-0787.

Stetson, K., Thompson, E., Donaldson, J. & Siler, L. 1983 Laminar boundary layer stability experiments on a cone at Mach 8, part 1: sharp cone. *AIAA Paper* 83-1761.